Clim Dyn (2017) 49:1765–1781
DOI 10.1007/s00382-016-3410-2

How will precipitation change in extratropical cyclones as the planet warms? Insights from a large initial condition climate model ensemble

Vineel Yettella[1] · **Jennifer E. Kay**[1]

Received: 22 March 2016 / Accepted: 15 October 2016 / Published online: 27 October 2016

Abstract The extratropical precipitation response to global warming is investigated within a 30-member initial condition climate model ensemble. As in observations, modeled cyclonic precipitation contributes a large fraction of extratropical precipitation, especially over the ocean and in the winter hemisphere. When compared to present day, the ensemble projects increased cyclone-associated precipitation under twenty-first century business-as-usual greenhouse gas forcing. While the cyclone-associated precipitation response is weaker in the near-future (2016–2035) than in the far-future (2081–2100), both future periods have similar patterns of response. Though cyclone frequency changes are important regionally, most of the increased cyclone-associated precipitation results from increased within-cyclone precipitation. Consistent with this result, cyclone-centric composites show statistically significant precipitation increases in all cyclone sectors. Decomposition into thermodynamic (mean cyclone water vapor path) and dynamic (mean cyclone wind speed) contributions shows that thermodynamics explains 92 and 95% of the near-future and far-future within-cyclone precipitation increases respectively. Surprisingly, the influence of dynamics on future cyclonic precipitation changes is negligible. In addition, the forced response exceeds internal variability in both future time periods. Overall, this work suggests that future cyclonic precipitation changes will result primarily from increased moisture availability in a warmer world, with secondary contributions from changes in cyclone frequency and cyclone dynamics.

Keywords Extratropical cyclones · Precipitation · Storm tracks · Climate variability · Initial condition ensembles

1 Introduction

Extratropical cyclones (hereafter cyclones) exert a strong influence on extratropical weather and climate. Cyclones control cloud amount and, as a consequence, radiation received by the extratropics. In addition, cyclones transport heat and moisture poleward and are an important part of the global atmospheric circulation. Of specific relevance to this study, cyclones produce a large fraction of extratropical precipitation. For example, Hawcroft et al. (2012) found cyclones contribute more than half of total Northern Hemisphere (NH) winter extratropical precipitation. Similarly, Catto et al. (2012) show that up to 90% of rainfall in the major storm-track regions is associated with fronts.

Recognizing the importance of cyclonic precipitation, an obvious question emerges: how will cyclonic precipitation change in a warming world? Previous work has addressed this question. For example, using an objective cyclone detection and compositing technique, Bengtsson et al. (2009) found that cyclone precipitation increased 11% per track over the twenty-first century, which is about twice the projected increase in global precipitation (Held and Soden 2006). Using a feature tracking algorithm, Zappa et al. (2013) investigated the response of North Atlantic and European extratropical cyclones to climate change in the climate models participating in phase 5 of the Coupled Model Intercomparison Project (CMIP5) and ascribed the uncertainty in cyclone precipitation response to the competing effects of

✉ Vineel Yettella
Vineel.Yettella@Colorado.EDU

[1] Cooperative Institute for Research in Environmental Sciences (CIRES) and Department of Atmospheric and Oceanic Sciences (ATOC), University of Colorado at Boulder, 216 UCB, Boulder, CO 80309, USA

increased moisture content and reduced cyclone intensity. Internal variability may be important for explaining precipitation differences amongst climate projections (Power et al. 2012), but internal variability uncertainty has been difficult to separate from model formulation uncertainty in previous studies using ensembles of opportunity such as CMIP5 (Tebaldi and Knutti 2007).

Building upon previous work, we analyze the influence of global warming on cyclonic precipitation in an initial condition ensemble of a global coupled climate model: the CESM Large Ensemble (CESM-LE, Kay et al. 2015). The CESM-LE consists of 30 realizations of a single model (CESM-CAM5, Hurrell et al. 2013) under the same external forcing. Ensemble spread is generated by small differences in initial conditions alone. The small initial condition differences grow and create spread among the ensemble members. Using the CESM Large Ensemble, we can for the first time robustly quantify cyclone-associated precipitation change in the presence of internal climate variability, albeit within a single modeling framework.

Our study has three specific goals. First, we quantify future changes in total and *cyclone-associated* extratropical precipitation in the CESM-LE. Specifically, we compare total and cyclone-associated precipitation in the present with that in the near- and far-futures and assess when the forced signal emerges above the internal climate variability using a simple statistical test. Second, we map precipitation rate changes within cyclones using cyclone-compositing. Finally, and most importantly, we assess the processes underlying projected changes in two quantities: *cyclone-associated* and *within-cyclone* precipitation. It is important to be clear about what these two terms mean. *Cyclone-associated* precipitation refers to the precipitation that accumulates at any grid point of interest due to cyclonic influence and in a sense is Eulerian in perspective. *Within-cyclone* precipitation refers to the precipitation occurring within individual cyclone systems and in a sense is Lagrangian in perspective.

Quantifying cyclone-associated and within-cyclone precipitation first requires identifying cyclones, a topic with a long history which we briefly introduce here. Early cyclone studies were limited by the lack of computing power. With the rise of computing power, and the advent of climate models and gridded analyses, the doors were opened for detailed objective studies of synoptic variability in the extratropics and the structure and evolution of individual cyclones. One of the earliest numerical studies of synoptic variability was done by Blackmon (1976), who used an Eulerian approach based on bandpass-filtered variance of the 500 hPa geopotential height. Feature-based Lagrangian techniques were also developed that identify and track individual cyclones. These techniques provide a more direct and clearer way of studying the structure and evolution characteristics of individual cyclones than provided by an Eulerian approach. These techniques differ in their choice of identification and tracking criteria which can sometimes lead to differences in the results obtained and inferences made (Neu et al. 2013). In this study, we adopt such a Lagrangian technique developed by Serreze (1995) for the identification of cyclone centers in all ensemble members but make no attempt to track them. We then extract the precipitation around identified cyclone-centers to estimate the contribution of cyclones to precipitation in the extratropics.

After identifying cyclone centers, quantifying future within-cyclone precipitation rate changes using a cyclone-compositing approach follows naturally and provides useful cyclone-centric information. Cyclone composites of precipitation are produced by averaging the cyclone-center relative precipitation fields of individual cyclones. Averaging smooths the variability in individual cyclone fields and reveals the structure present in a typical cyclone. The compositing approach has been used in a host of studies ranging from the observation-based investigation of precipitation and cloud structure in cyclones (Lau and Crane 1995; Field and Wood 2007; Naud et al. 2012) to the evaluation of the reproduction of certain aspects of cyclones by climate models (Klein and Jakob 1999; Bauer and Del Genio 2006; Field et al. 2008; Bodas-Salcedo et al. 2012). By comparing the ensemble mean composites in the present with those in the near- and far-futures, we unveil the magnitude and pattern of precipitation change in cyclones.

Quantifying precipitation change is the first step, but understanding the mechanisms underlying projected changes in cyclonic precipitation is the most important goal of this study. Such an evaluation is particularly relevant in the context of the expected increase in atmospheric moisture content (Held and Soden 2006) and the poleward shift of the cyclone tracks with global warming (Yin 2005). We ask two questions in this context: (1) How do changes in frequency of cyclones affect cyclone-associated precipitation? and (2) What factors cause future changes in within-cyclone precipitation?

We organize the paper as follows: In Sect. 2, we detail our cyclone identification and compositing procedures and decomposition methods. In Sect. 3, we present our results addressing the primary goals of our study: quantifying and explaining. In Sect. 4, we place our results into a broader context and finally, in Sect. 5, we summarize. As we will show, our study highlights the important role that thermodynamics plays in controlling the future precipitation within extratropical cyclones and the negligible effect internal climate variability has on the cyclonic precipitation response to global warming.

2 Methods

2.1 Initial condition ensemble: the CESM large ensemble

To quantify future changes in the presence of internal variability, we utilize daily averaged output from the CESM-LE: an ensemble of 30 CESM1-CAM5 simulations at 1° × 1° resolution. The 30 CESM-LE simulations were carried out for the period 1920–2100 under identical external forcing but starting from slightly different initial conditions. Historical forcing was applied from 1920 to 2005 and Representative Concentration Pathway 8.5 (RCP 8.5) forcing was used from 2006 to 2100. The first ensemble member was started using January 1 conditions of a randomly selected year (402) of a 1500-year pre-industrial (defined as 1850) control run of CESM1-CAM5 and then integrated forward from 1850 to 2100. The state of the first ensemble member on Jan 1, 1920 was used to initialize the rest of the ensemble members. A small random perturbation (order of 10^{-14} K) to the initial air temperature field was added to each ensemble member before integrating them forward from 1920 to 2100. Due to the chaotic nature of the climate system, these perturbations grow until initial condition memory is lost creating spread among ensemble members. A detailed description of the CESM-LE can be found in Kay et al. (2015).

Using the CESM-LE, we compute precipitation responses in two seasons: DJF and JJA. Following the IPCC, we define the present, near-future and far-future as 1986–2005, 2016–2035, 2081–2100 respectively. We compute the precipitation response as ensemble-mean epoch differences between the future epochs and the present. Assuming ensemble members to be independent, we evaluate the 95% statistical significance of the responses against a null hypothesis of zero change using a 2-sided student *t* test.

2.2 Analysis methods used

2.2.1 Cyclone identification and compositing

Cyclone centers are identified as minima in the daily averaged sea level pressure (PSL) fields following the methodology outlined in Serreze (1995). Keeping in mind the large amount of data to be processed, we have refrained from using other, more computationally expensive cyclone identification methods, for example, those based on vorticity (Hoskins and Hodges 2005). Prior to the identification, PSL fields are smoothed in space using four passes of a nine-point local smoother. Smoothing eliminates a majority of spurious lows produced near high topography due to incorrect model extrapolation to sea level. Grid points in the extratropical regions (defined as the latitude bands between 30° and 90° in both hemispheres) with a PSL value lower than the values at the surrounding 8 points are then identified as minima. After identification, the central PSL values are compared with PSL values at surrounding grid cells in a series of outwardly expanding shells. Minima are then filtered based on threshold PSL values at these shells. Applying these filtering criteria eliminates weak depressions as well as spurious lows that survive the smoothing procedure. Minima that pass the filtering procedure are considered cyclone centers and their locations, date of occurrence and central pressure are entered into a dataset. The total number of cyclone centers detected globally in all time periods and all ensemble members stood at approximately 6,600,000 which is an average of 10 cyclone centers per day globally in each ensemble member.

No attempt is made to construct cyclone tracks using the identified cyclone centers. Tracking proved difficult using the daily averaged CESM-LE data available to us. In 24 h, cyclones can travel a distance which is on the same order as the separation between individual systems. This can lead to false associations between cyclone centers on consecutive days. For this reason, each cyclone on each day is treated as an individual system. This approach has been used in other studies as well (Lambert and Fyfe 2006; Finnis et al. 2007).

We now describe the cyclone compositing procedure. Compositing has been used in various studies to calculate the average structure of cyclonic variables (Field and Wood 2007; Bodas-Salcedo et al. 2012; Hawcroft et al. 2012, their appendix). Composites can be produced by simply using the latitude-longitude grid to define cyclonic area around each center. However, this can introduce bias due to grid distortion especially in the extratropics. This problem can be avoided by using a natural radial grid centered on each cyclone center (Bengtsson et al. 2007). We define a radial grid (Appendix section) of great radius 2000 km with 100 km shell spacing. Each shell consists of 360 equally spaced points. Model fields of any desired meteorological variable (in this paper wind velocities, precipitation and SLP) at any desired height (in this paper at the surface) are bilinearly interpolated onto the radial grid. Composites are then produced by averaging these radial fields.

2.2.2 Decomposition of cyclone-associated precipitation change at grid points

Following Zappa et al. (2014), we decompose cyclone-associated precipitation change at each grid point into contributions from changes in the number of days cyclones are present in the neighborhood of the grid point and average precipitation rate change in those cyclones. The "neighborhood" is defined as a 2000 km radial cap centered on the grid point. The methodology works as follows: Let P(x, y)

be a grid point. Let N_1 be the total number of days in which cyclones are present in the neighborhood of P(x, y). The total cyclone contributed precipitation at that grid point can then be represented by:

$$P_C = N_1 \cdot \mu_1 \tag{1}$$

where μ_1 is the mean precipitation that falls at the grid point during the N_1 days. The change in P_C in a future time period can then be written as

$$\delta P_C = (N_2 - N_1)\mu_1 + (\mu_2 - \mu_1)N_1 + (N_2 - N_1)(\mu_2 - \mu_1) \tag{2}$$

where N_2 and μ_2 are the equivalents of N_1 and μ_1 for a future time period. The first term on the RHS is interpreted as the contribution from changes in the fraction of time the grid point spends in the neighborhood of cyclones. The second term is interpreted as the contribution from changes in the precipitation rate in cyclones. The third term represents covariation.

As mentioned in Hawcroft et al. (2012), total cyclone-associated precipitation is sensitive to the size of the radial cap that is selected. Hawcroft et al. (2012) chose 12° (1334 km)/10° (1120 km) radial caps for DJF/JJA for extracting cyclonic precipitation based on an investigation into the behavior of average cyclonic precipitation as a function of distance from the cyclone center. We chose a 2000 km radial cap for both seasons based on a similar investigation (not presented in the paper). The larger cap size is a consequence of our choice of cyclone identification method as well as using daily-averaged data which spatially smooths out the precipitation field. In our investigation, we found that the frontal precipitation band can be offset from the pressure low by as much as 500 km which meant that a larger cap had to be used to capture all of this precipitation. A sensitivity test using various cyclone radii showed that our results are robust to the choice of cyclone radius.

2.2.3 *Decomposition of precipitation change in cyclones*

Using a simple mass conservation argument, Field and Wood (2007) showed that the warm conveyor belt (WCB) rain rate R_{WCB} in a cyclone is proportional to the product of cyclonewide-averaged surface wind speed (V) and cyclonewide-averaged column-integrated water vapor (Water Vapor Path WVP):

$$R_{WCB} \propto V \cdot WVP \tag{3}$$

Pfahl and Sprenger (2016) show that this relationship explains a large fraction of the variance of cyclone precipitation at all latitudes. Because most cyclonic precipitation occurs in the WCB, Eq. (3) still holds if R_{WCB} were replaced by the cyclonewide-averaged precipitation rate PR. Since PR is simpler to calculate, we use it as a substitute for R_{WCB}. We adopt V and WVP as measures of the strength and moisture content of a cyclone respectively. We also assume the two quantities to be independent based on the arguments of Field and Wood (2007). V, WVP and PR are calculated for each cyclone center on a 2000 km radial grid centered on the cyclone center (see previous section) with cosine weighting to account for the clustering of points towards the center of the radial grid (see Fig. 14 in Appendix).

We next describe the decomposition procedure. Consider a set of cyclones C_P detected in a desired region and time period. Let C_F be the set of cyclones detected in the same region in a future time period. Let $\langle PR \rangle_{P(F)}$ be the mean PR value of cyclones in $C_{P(F)}$. $\langle PR \rangle_F - \langle PR \rangle_P$ then represents future change in the mean of cyclonewide-averaged precipitation of cyclones occurring in that region. The decomposition procedure splits this change into contributions from future changes in the strength and moisture content of cyclones in that region. The first step in the procedure is to construct probability density functions (PDFs) of V in each set by binning. Let these PDFs be denoted by Pv_P and Pv_F corresponding to C_P and C_F respectively. Each bin represents a distinct cyclone strength regime. Into each bin, PR values from C_P are composited to obtain a distribution of PR conditioned on V and denoted by F_P. The conditional distribution F_F corresponding to C_F is obtained in the same way. $\langle PR \rangle_F - \langle PR \rangle_P$ can then be represented:

$$\langle PR \rangle_F - \langle PR \rangle_P = \sum_{i=1}^{k} F_{P_i}\left(Pv_{F_i} - Pv_{P_i}\right) + \sum_{i=1}^{k}\left(F_{F_i} - F_{P_i}\right)Pv_{P_i} + \sum_{i=1}^{k}\left(F_{F_i} - F_{P_i}\right)\left(Pv_{F_i} - Pv_{P_i}\right) \tag{4}$$

where k is the number of bins and the index i indicates evaluation in the ith bin.

The first term on the right hand side of Eq. (4) represents the change in $\langle PR \rangle$ due to future change in the PDF of V with the distribution of PR conditioned on V remaining unchanged. It is interpreted as the result of changes in the average strength of cyclones in the region. The second term is the change in $\langle PR \rangle$ due to future change in the distribution of PR conditioned on V with the PDF of V remaining unchanged. It is interpreted as the result of changes in the average moisture content of cyclones in the region. The third term represents covariation. This simple decomposition framework was used by Emori and Brown (2005) to split precipitation change into contributions from changes in dynamic and thermodynamic components at individual grid points and by Bony et al. (2004) to infer dynamic and thermodynamic components of cloud response to climate variations.

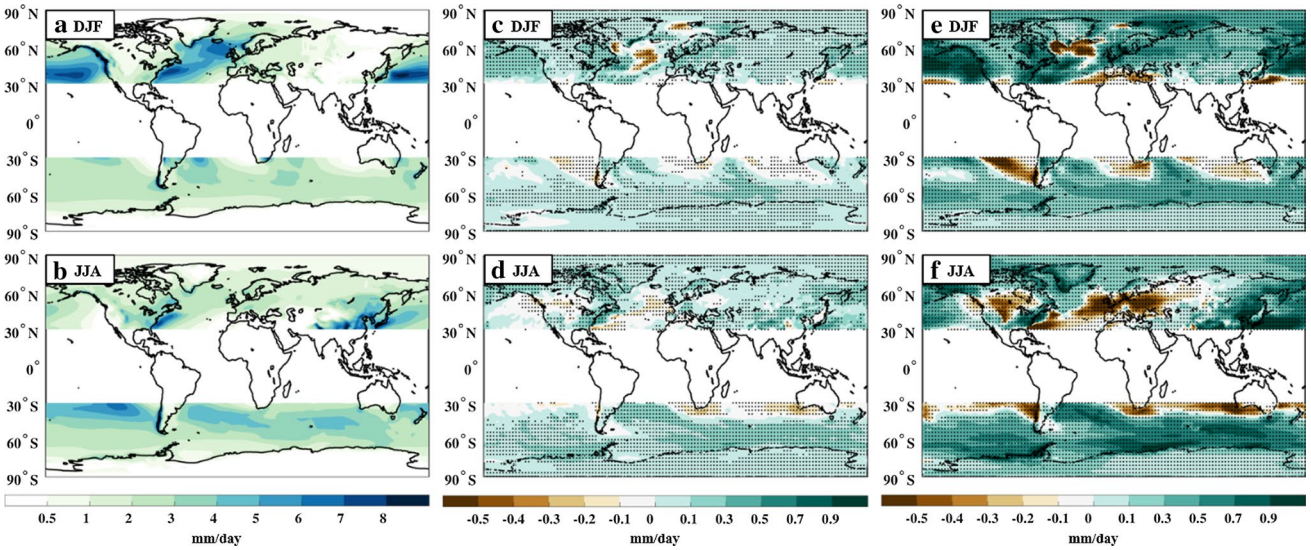

Fig. 1 Ensemble-mean extratropical precipitation (EP): **a** DJF Present day (1986–2005), **b** JJA present day, **c** DJF near-future (2016–2035), **d** JJA near-future, **e** DJF Far-future (2081–2100), **f** JJA far-future. Stippling indicates statistically significant change at the 95% confidence level

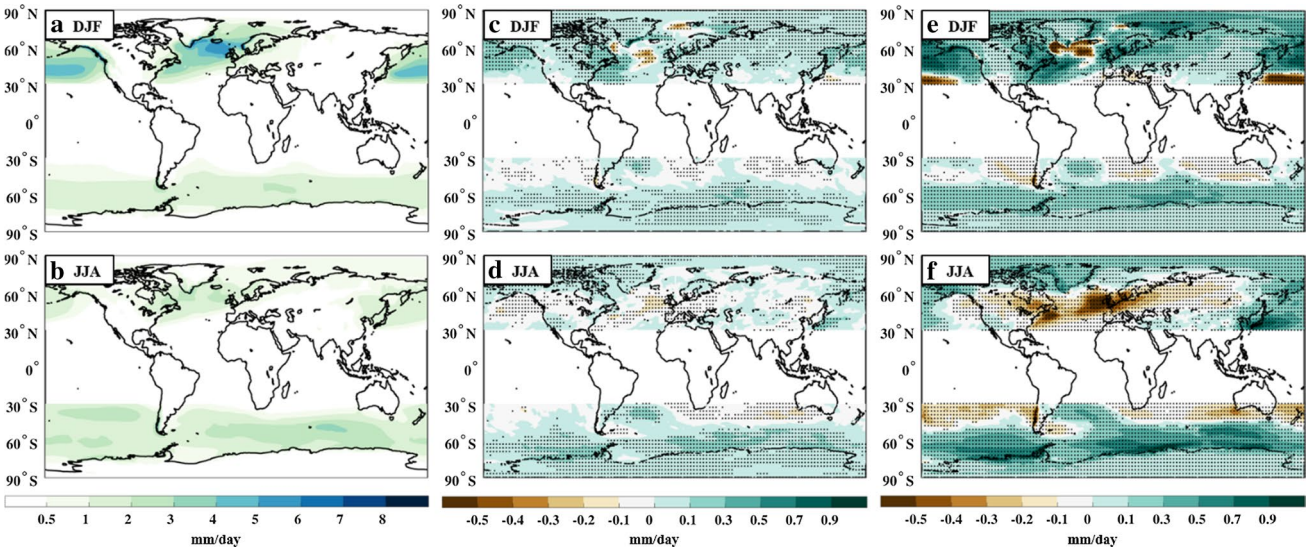

Fig. 2 Ensemble-mean cyclone-associated precipitation (CP): **a** DJF Present day (1986–2005), **b** JJA present day, **c** DJF near-future (2016–2035), **d** JJA near-future, **e** DJF Far-future (2081–2100), **f** JJA near-future. Stippling indicates statistically significant change at the 95% confidence level

3 Results

3.1 Precipitation: present day and future changes

We begin by presenting present-day and future changes in extratropical precipitation within the CESM-LE. For ease of comparison with previous work, we examine changes in two seasons: DJF and JJA. We focus on the ensemble mean to minimize noise from internal climate variability. The largest present-day extratropical precipitation rates occur over the ocean basins in the storm track regions where the precipitation rates approach 8 mm/day (Fig. 1a, b). The contribution of cyclones to extratropical precipitation generally agrees well with the observations-based results of Hawcroft et al. (2012) (see their Figs. 2, 3). However, we caution that such a comparison could be compromised by differences in cyclone identification methodologies. For example, the contribution over the continental United

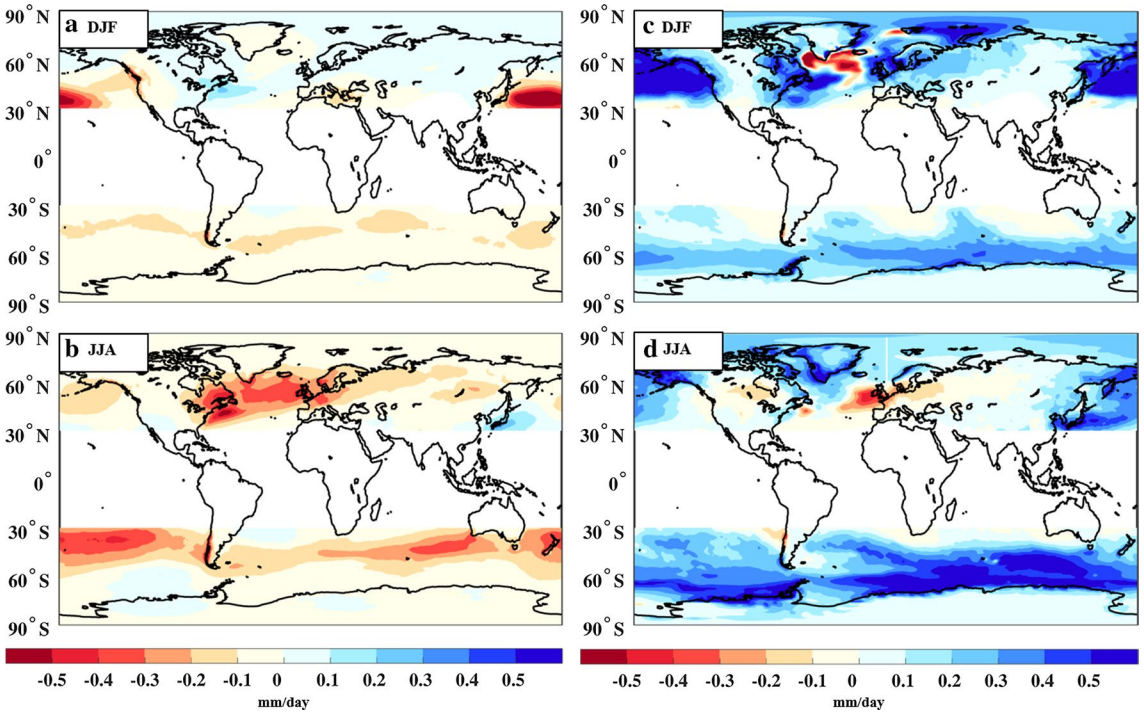

Fig. 3 Contributions to cyclone-associated precipitation (CP) changes in the far-future (2081–2100): **a** DJF cyclone frequency change contributions, **b** JJA cyclone frequency change contributions, **c** DJF within-cyclone precipitation change contributions, **d** JJA within-cyclone precipitation change contributions

States is underestimated, in some places by as much as 30%.

Both the near-future and the far-future precipitation responses are statistically significant over the majority of extratropics (Fig. 1c–f). While the magnitude of the precipitation change is larger in the far-future than in the near-future, both future periods have similar spatial patterns of precipitation change. During both the near-future and the far-future, precipitation increases when compared to the present in most extratropical regions.

We next focus on cyclone-associated precipitation in the CESM-LE. Similar to the total precipitation, the majority of cyclone-associated precipitation occurs in oceanic storm tracks in both DJF and JJA (Fig. 2a, b). Indeed, similar patterns of total precipitation (Fig. 1a, b) and cyclone-associated precipitation (Fig. 2a, b) demonstrate cyclonic activity is the dominant control on mid-latitude precipitation in the CESM-LE. Consistent with seasonal variations in NH cyclonic activity, NH cyclonic precipitation is larger in NH winter (DJF) than in NH summer (JJA). While more cyclonic precipitation also occurs in SH winter (JJA) than in SH summer (DJF), the seasonal variations in cyclonic precipitation are smaller in the SH than in the NH.

Having demonstrated that cyclones are a primary contributor to present-day extratropical precipitation in the CESM-LE, it follows that the spatial pattern of cyclonic precipitation change (Fig. 2c–f) closely matches the total precipitation change (Fig. 1c–f). Also similar to the total precipitation future change pattern, the cyclonic precipitation change pattern intensifies in the far-future with more grid points experiencing statistically significant changes.

3.2 Decomposition of future changes in cyclonic precipitation at individual grid points

Two factors explain future cyclone-associated precipitation changes in a warming world—contributions from changes in cyclone frequency and contributions from changes in within-cyclone precipitation (see methods in Sect. 2.2.2). We compare these contributions in Figs. 3 and 4. Within-cyclone precipitation change contributions dominate cyclone frequency change contributions in most regions. In most of the extratropics, within-cyclone precipitation change contributions increase cyclone-associated precipitation. Notable exceptions are the decreases seen over the North Atlantic and the Mediterranean region in DJF and over North America and Western Europe in JJA (Figs. 3c, d, 4c, d). While within-cyclone precipitation change contributions are first-order, cyclone frequency change contributions do have a comparable magnitude over a considerable area of the extratropics. Particularly noticeable are the decreases seen over the Pacific storm track in DJF and over

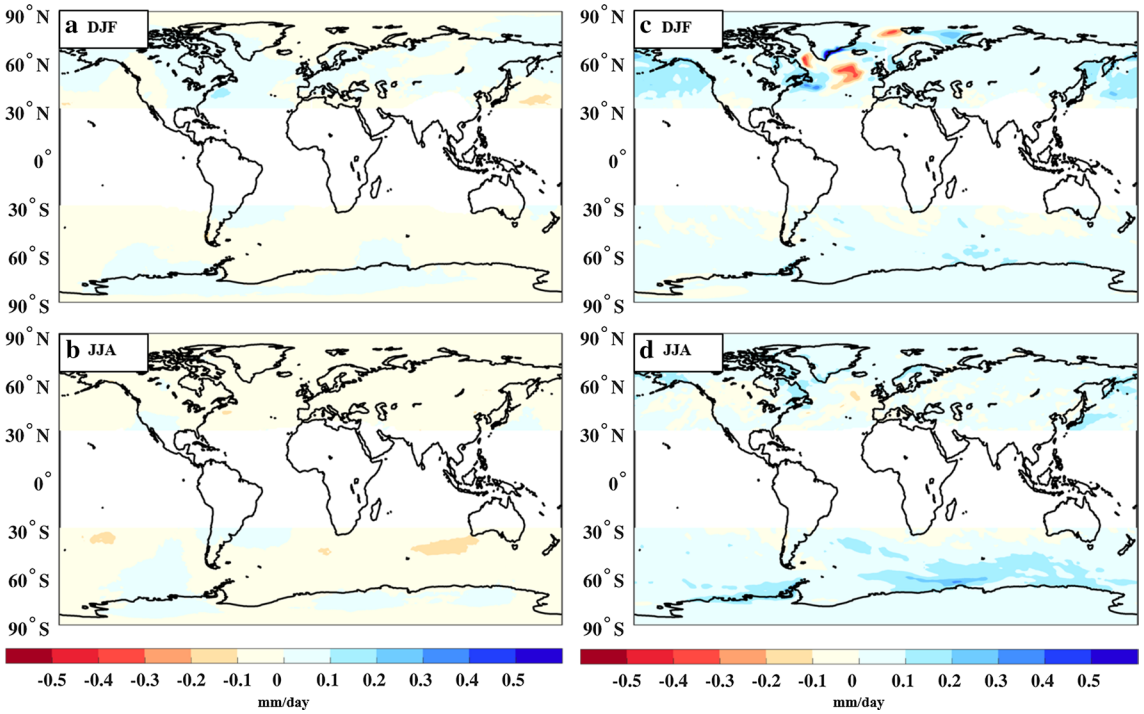

Fig. 4 As in Fig. 3 but for the near-future (2016–2035)

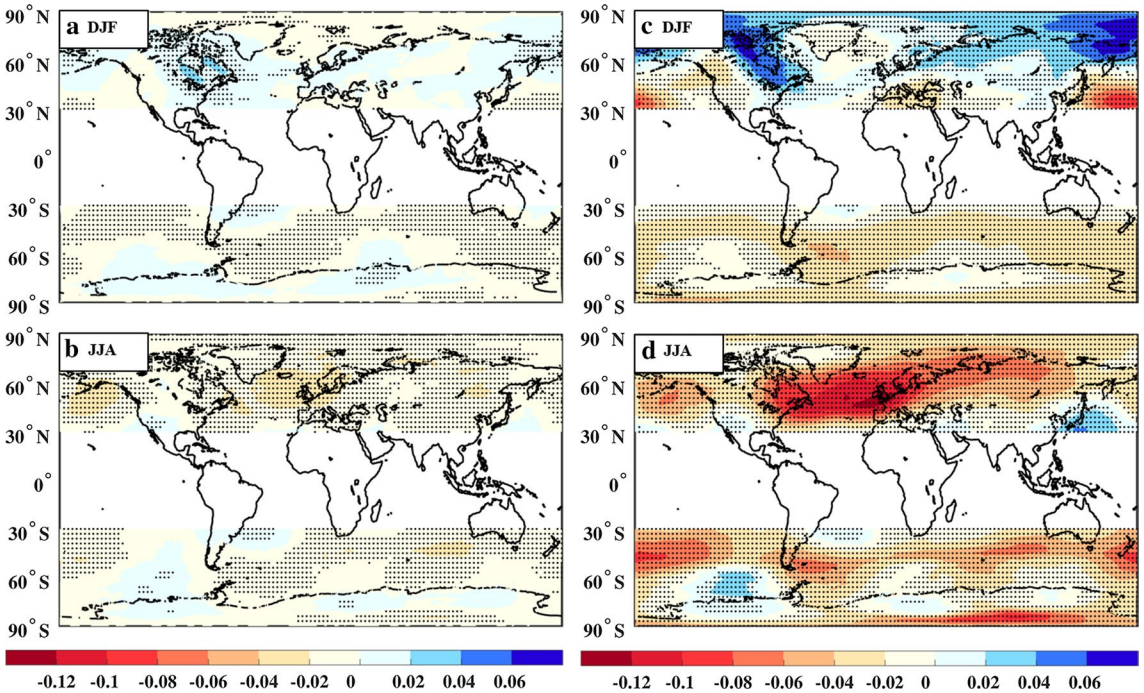

Fig. 5 Future changes in the fraction of time that a grid point spends under cyclonic influence: **a** DJF near-future (2016–2035) changes, **b** JJA near-future changes, **c** DJF far-future (2081–2100) changes, **d** JJA far-future changes. Stippling indicates statistically significant change at the 95% confidence level

the North Atlantic in JJA (Figs. 3a, b, 4a, b), consistent with future cyclone frequency changes (Fig. 5).

3.3 Precipitation composites

Having learned that within-cyclone precipitation changes dominate over cyclone frequency changes throughout most of the extratropics, we next further examine within-cyclone precipitation changes using composites of present-day cyclonic precipitation and future changes. We start with cyclone composites of precipitation by hemisphere and season (Fig. 6). The comma-shaped precipitation structure associated with the warm conveyer belt is clearly visible in the composites. The comma shape is flipped in the SH

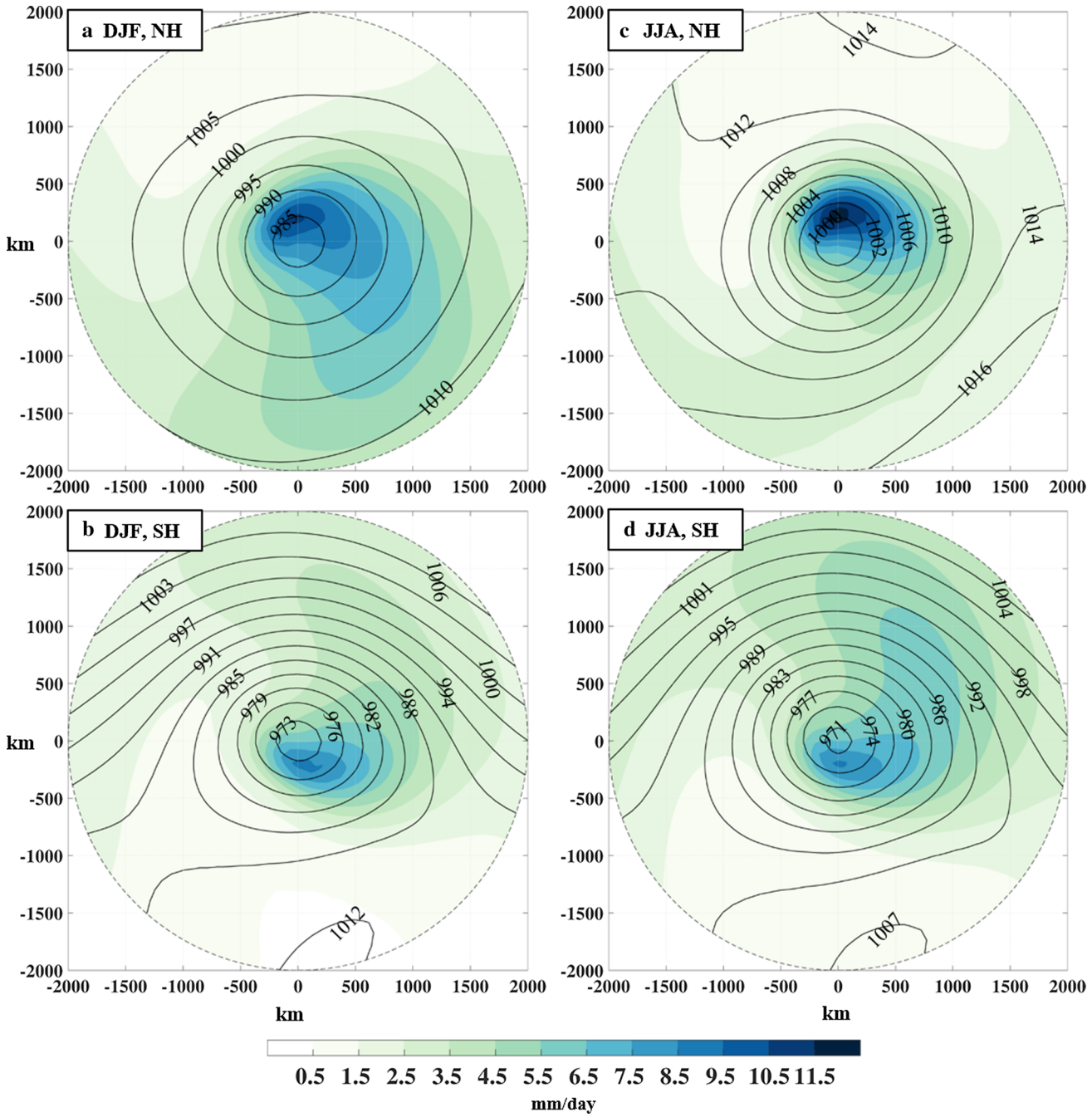

Fig. 6 Present-day (1986–2005) ensemble-mean cyclone precipitation composites: **a** DJF composite in the Northern Hemisphere (NH), **b** DJF composite in the Southern Hemisphere (SH), **c** as in **a** but for JJA, **d** as in **c** but for SH. Precipitation is plotted in *colored contours*. Mean PSL (hPa) is overlaid as *black contour lines*

composites (Fig. 6b, d). In both the SH and NH composites, precipitation reaches its greatest intensity close to the cyclone center. The composites are constructed by averaging the radial precipitation fields from a few hundred-thousand cyclones contributed by all ensemble members. Hence they represent greatly averaged precipitation footprints. The individual precipitation footprints of the cyclones were found to be highly variable. The composites represent the spatial average extent of cyclonic precipitation. The extent found in the composites justifies the selection of a 2000 km radial cap—it captures most of the cyclonic precipitation. The precipitation magnitude in the central regions of the composites agrees well with that in the composites derived from observational data (Hawcroft et al. 2012, their Figure S1; Field and Wood 2007, their Figure 3). The comma shape of the precipitation band matches the composites in Field and Wood (2007) in terms of its spatial spread and orientation.

We next show precipitation change in cyclone composites of the future compared with the present (Figs. 7, 8). In all composites, statistically significant precipitation increases occur at most points on the radial grid. The greatest precipitation increases occur near the composite centers, also where the cyclone precipitation is largest. The rate of change of saturation vapor pressure with change in temperature is highest in NH, JJA. Correspondingly, we see the greatest increases in the NH, JJA composites suggesting a strong role for thermodynamics in cyclone precipitation change.

3.4 Decomposition of future changes in precipitation within cyclones

Our results thus far reveal that within-cyclone precipitation in both hemispheres increases in the future (Figs. 7, 8). A next obvious question is: Why is precipitation increasing within the cyclone composites in a warming world? To answer this question, we decompose precipitation changes into contributions from the changes in the cyclones' thermodynamic and dynamic environments.

We quantify in every ensemble member, the contribution of changes in the moisture content and wind speed of cyclones to future changes in precipitation within cyclones (Fig. 9; methods described in Sect. 2.2.3). Contributions from increases in moisture content dominate those from changes in wind speed and increase $\langle PR \rangle$ in all ensemble members irrespective of the ensemble member and time period. On average, increase in moisture accounts for more than 90% of within-cyclone precipitation increase in both future time periods (Table 1). In contrast, the contribution from changes in wind speed are smaller. The covariance terms are negligible in all cases. In agreement with the negligible contribution of changes in dynamics, future cyclonic V PDFs vary little compared with those in the present (Fig. 10a). In contrast, a clear shift to higher values can be seen in future WVP PDFs (Fig. 10b). Interestingly, the number of cyclones with extreme values of moisture content increases at the expense of the number of cyclones with moderate moisture content.

We next map the contributions of moisture content and wind speed to precipitation changes in the two future periods (Figs. 11a–d, 12a–d). Since the decomposition is performed utilizing sets of cyclones in a 2000 km radius around each grid point, the figures display a spatially smoothed map of the contributions. In general, the thermodynamic contributions (Figs. 11c, d, 12c, d) increase $\langle PR \rangle$. In contrast to this general rule, thermodynamic changes reduce $\langle PR \rangle$ in the lower parts of North America and the Mediterranean region during JJA (Figs. 11d, 12d). Unlike thermodynamic contributions, dynamic contributions have a mixed influence on $\langle PR \rangle$ (Figs. 11a, b, 12a, b). Interestingly, the dynamic contribution changes sign over a major portion of the Northern extratropics between the near- and far-futures. In most regions in the far-future, the dynamic contribution is considerably smaller than the thermodynamic contribution. An exception is in the North Atlantic and in the subsidence regions, where the dynamic and thermodynamic components have comparable magnitudes in both seasons.

We now examine mean within-cyclone precipitation changes (Fig. 13) that contribute to cyclone-associated precipitation changes (Figs. 3c, d and 4c, d). These changes do not always correlate positively with their contributions to cyclone-associated precipitation changes. Within-cyclone precipitation changes are significant in most regions of the extratropics in both epochs and seasons. The contours follow those of the thermodynamic contributions (Figs. 11c, d, 12c, d), highlighting the importance of increased moisture content in a warming world for driving increased cyclonic precipitation.

4 Discussion

Despite the potential for complexity, we found modeled precipitation changes in extratropical cyclones in a warming world are simple to explain: precipitation increases because water vapor increases. Using the classic warm conveyer belt model and the finding that the cyclone strength change is negligible (Figs. 10a, 11a, b, 12a, b), most of the increase can be attributed to increased moisture content in a warmer atmosphere. This result agrees with Li et al. (2014) who used recent warm periods in reanalysis data as analogues for future warming and found increased cyclonic precipitation but essentially unchanged cyclone intensity. Cyclone compositing also revealed that increased water vapor availability leads to increased precipitation in the central regions of model cyclones.

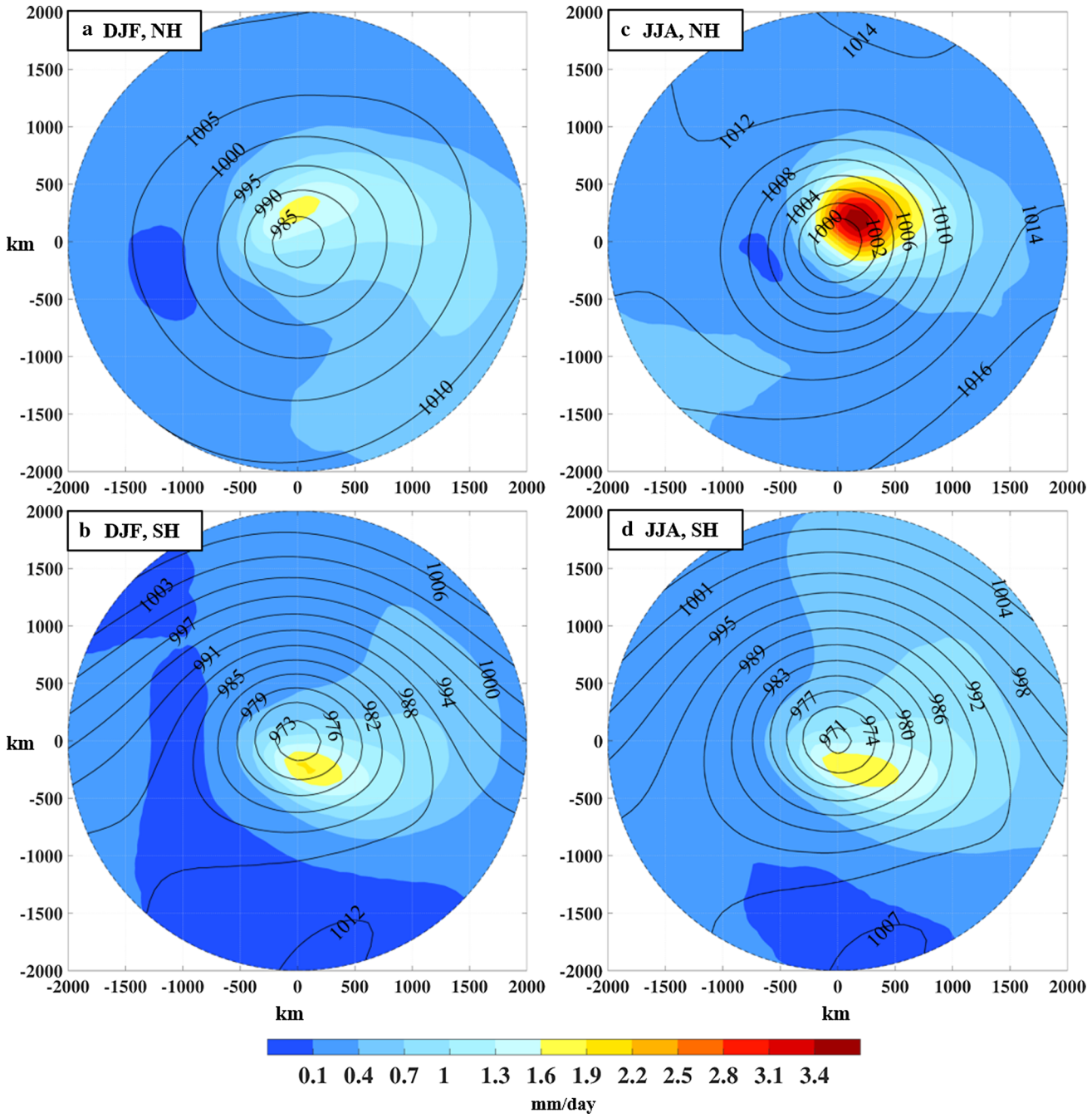

Fig. 7 Far-future (2081–2100) ensemble-mean cyclone precipitation difference composites. **a** DJF difference composite in the Northern Hemisphere (NH), **b** as in **a** but for the Southern Hemisphere (SH), **c** as in **a** but for JJA, **d** as in **c** but for SH. Precipitation difference is plotted in colored contours. Present-day (1986–2015) mean PSL (hPa) is overlaid as *black contour lines*. All regions are statistically significant at the 95% level

There are regional exceptions to our overall finding that thermodynamics increases within-cyclone precipitation. For example, changes in thermodynamics considerably reduce within-cyclone precipitation over South-Central Europe and over a major portion of the United States in the far-future (Fig. 12d). This reduction occurs despite of increased average cyclone moisture content and only slightly decreased average cyclone strength in those regions (not shown). This suggests that within-cyclone precipitation simulated by the climate model in these regions is less than that predicted by the WCB model which warrants investigation.

All things considered, changes in cyclone dynamics are often negligible (Figs. 10a, 11a, b, 12a, b). As argued

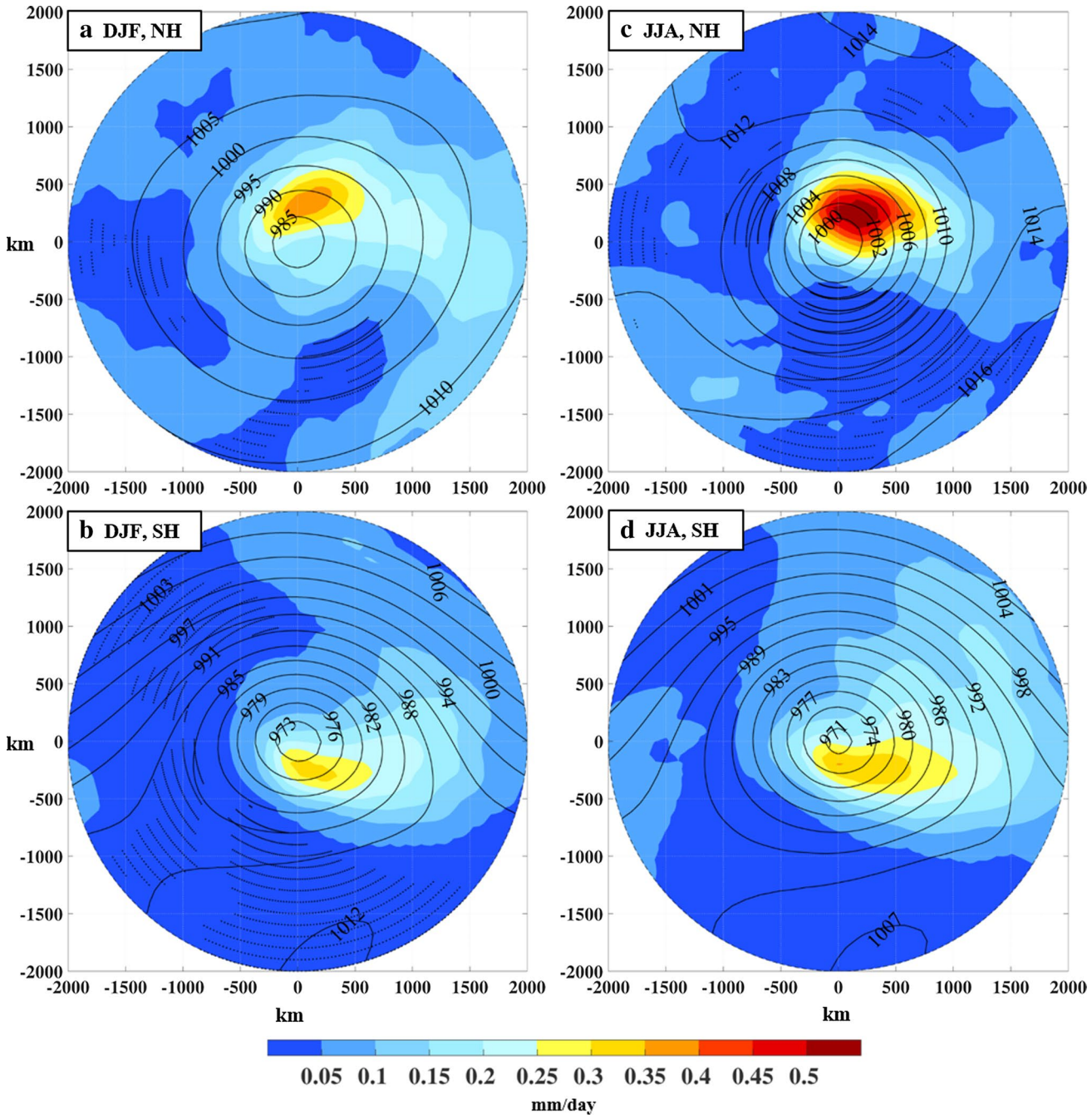

Fig. 8 As in Fig. 7 but for the near-future (2016–2035). Stippling indicates statistically insignificant change at the 95% confidence level

by Bengtsson et al. (2009), unchanging cyclone dynamics could be a result of compensation between the strengthening of storms due to increased moisture and an associated greater latent heating and the weakening of storms due to weakened equator to pole surface temperature gradient with a warming climate. We caution that this result might be resolution dependent. Cyclone intensity, in terms of surface wind speed, can increase, albeit modestly, in a warmer climate at finer resolutions (Booth et al. 2013).

This study also investigated the influence of changes in storm-frequency on cyclone-associated precipitation. Changes in storm-frequency in the future are consistent with results from literature. For example, in the far-future (Fig. 5c, d), SH cyclone frequency exhibits a dipole behavior by increasing in the Southern ocean (South of 60°S) and decreasing in the sub-Antarctic ocean (North of 60°S) agreeing with the results of Fyfe (2003). This dipole behavior also agrees with model projections of poleward SH

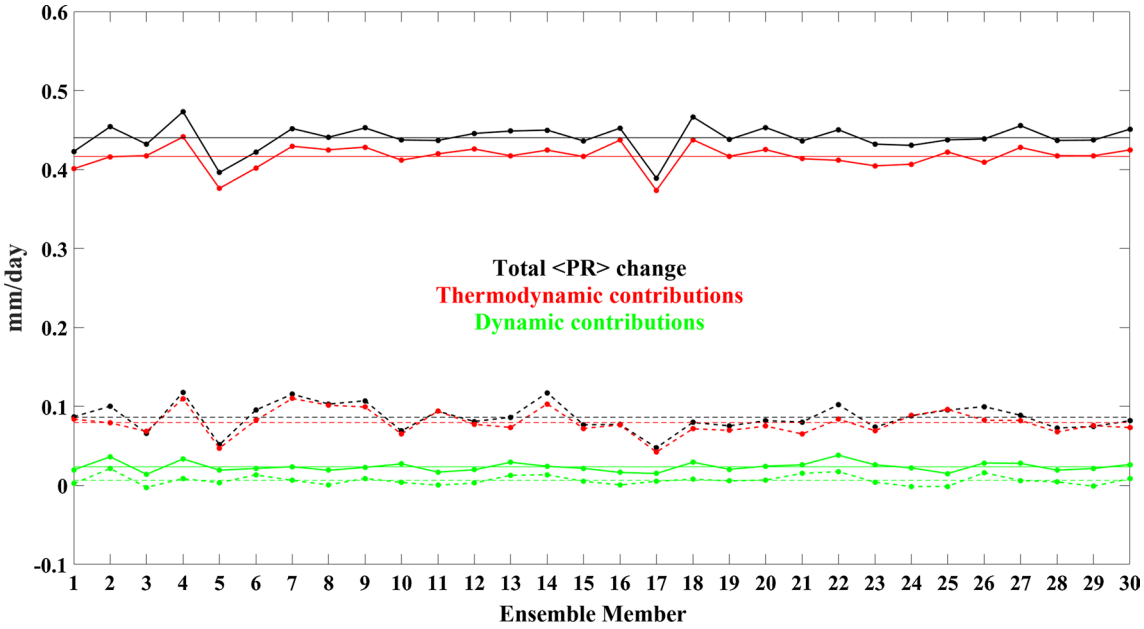

Fig. 9 Contributions to within-cyclone precipitation change. Near-future (2016–2035, *dash*). Far-future (2081–2100, *solid*). *Black*, *red* and *green* represent total mean cyclonewide-averaged precipitation (⟨PR⟩) changes, thermodynamic and dynamic contributions to ⟨PR⟩ changes respectively. *Horizontal lines* represent respective means (see Table 1 for values). Changes are calculated using methods in Sect. 2.2.3 for cyclones detected in the entire extratropical region (30°N(S)–60°N(S)) for DJF and JJA combined

Table 1 Ensemble mean contributions

	Near-future (2016–2035)	Far-future (2081–2100)
Total ⟨PR⟩ change (mm/day)	0.0863 (0.0173)	0.4402 (0.0174)
Thermodynamic contribution (mm/day), % of ⟨PR⟩ change	0.0796 (0.0160), 92%	0.4166 (0.0151), 95%
Dynamic contribution (mm/day), % of ⟨PR⟩ change	0.0066 (0.0061), 8%	0.0233 (0.0060), 5%

Standard deviation given in parentheses. Individual member values in Fig. 9. Methods in Sect. 2.2.3

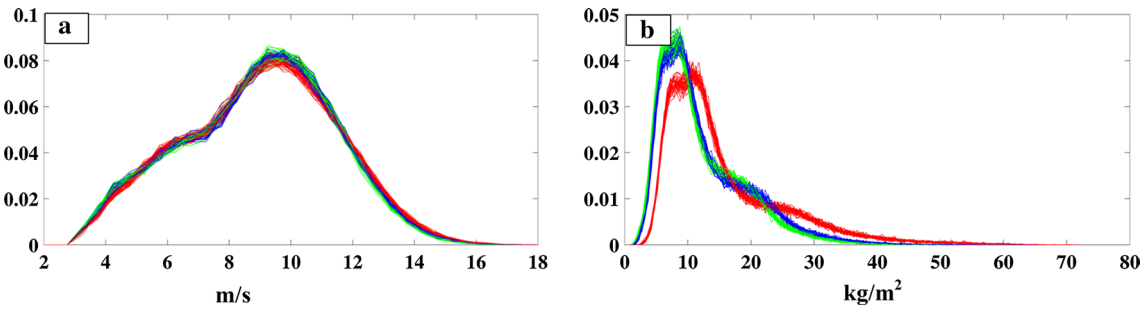

Fig. 10 Probability distribution functions of **a** cyclone-averaged wind speed V, **b** cyclone-averaged water vapor path WVP. *Green* present (1986–2005), *blue* near-future (2016–2035), *red* far-future (2081–2100). Individual *lines* represent ensemble members. The PDFs are derived for cyclones detected in the entire extratropical region (30°N(S)–60°N(S)) for DJF and JJA combined

storm track shifts. The dipole is stronger in JJA than in DJF due to the competing effect of ozone recovery in DJF which tends to oppose the poleward shift (Polvani et al. 2011). In boreal winter (Fig. 5c), the shifts are not necessarily poleward in all regions. For example, a tripolar response, as found in a multimodel assessment by Zappa et al. (2013),

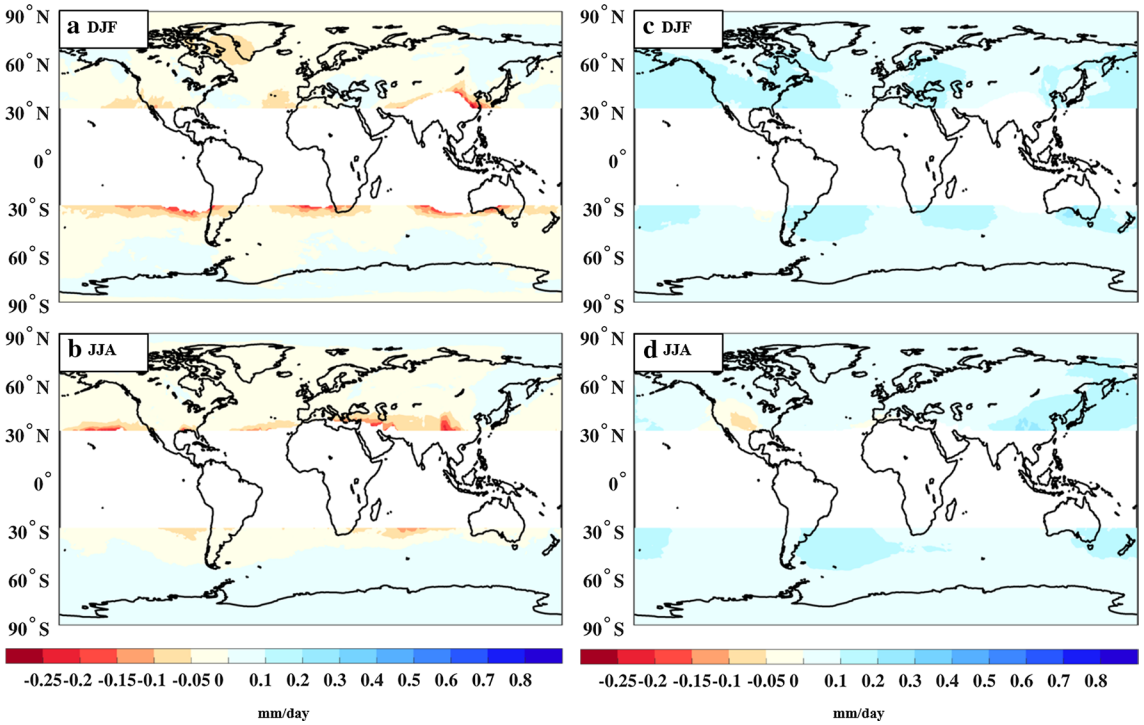

Fig. 11 Contributions to mean cyclone-wide averaged precipitation (⟨PR⟩) changes in the near-future (2016–2035). **a** DJF dynamic contributions, **b** JJA dynamic contributions, **c** DJF thermodynamic contributions, **d** JJA thermodynamic contributions. These maps were produced by constructing circles of great radius 2000 km at every grid point and applying the decomposition procedure described in Sect. 2.2.3 to the set of V, WVP and PR values of cyclones located within each *circle* in each ensemble member. The ensemble-mean of the resulting values of the contributions are assigned to the corresponding central grid point

is present over the North Atlantic Ocean and Europe, consistent with minimal jet shifts found by Barnes and Polvani (2013) in that region. In the North-Eastern Pacific however, clear poleward storm track shifts are present, as also noted by Barnes and Polvani (2013). In agreement with the findings of Chang et al. (2015), the gradient of frequency change over the East Pacific just off the North American coast suggests a southward shift of cyclones in that region. Contrary to their results however, cyclone activity in reduced. Consequently, the cyclone-associated precipitation increase over the coastal East Pacific and California regions (Fig. 2e) is explained exclusively by the increased precipitation intensity within cyclones (Fig. 3c). In boreal summer (Fig. 5d), cyclone frequency decreases throughout the extratropics, most prominently over the North Atlantic Ocean and Europe. The gradient of change is consistent with a clear poleward jet shift in those regions (Barnes and Polvani 2013). On comparing the contributions of changes in cyclone frequency and precipitation intensity (Figs. 3, 4) with total cyclonic precipitation change (Fig. 2c–f), the only regions where contributions by changes in cyclone frequency dominate are the winter time Pacific Storm tracks and SH low latitudes in addition to the summer time North Atlantic Ocean. In all other regions, contributions by changes in precipitation intensity associated with the increased moisture content clearly dominate during both seasons suggesting a stronger role for thermodynamics in causing cyclone-associated precipitation change. We caution that these results are specific to CESM-CAM5 and there is intermodel spread in the storm track response (Chang et al. 2012; Harvey et al. 2012).

In spite of the complex interaction between various physical drivers of change that could result in cyclone response uncertainty (Zappa et al. 2013, Woollings et al. 2010), our results under RCP 8.5 forcing show that the dominance of thermodynamics over dynamics rises above internal variability in both time periods (Fig. 9; Table 1). Even in the near future when internal variability noise can possibly hide signals from the forced response, the conclusion is very clear: changes in thermodynamics are far more important than changes in dynamics from a cyclone precipitation perspective. The relative magnitude of the ensemble spread in the contributions (standard deviations in Table 1) suggest that the role of internal variability is negligible and a small number of ensemble members is sufficient to detect the forced response in cyclones in an average sense even in the near-future. Ensemble spread in the contributions arising from internal variability was found to be minimal

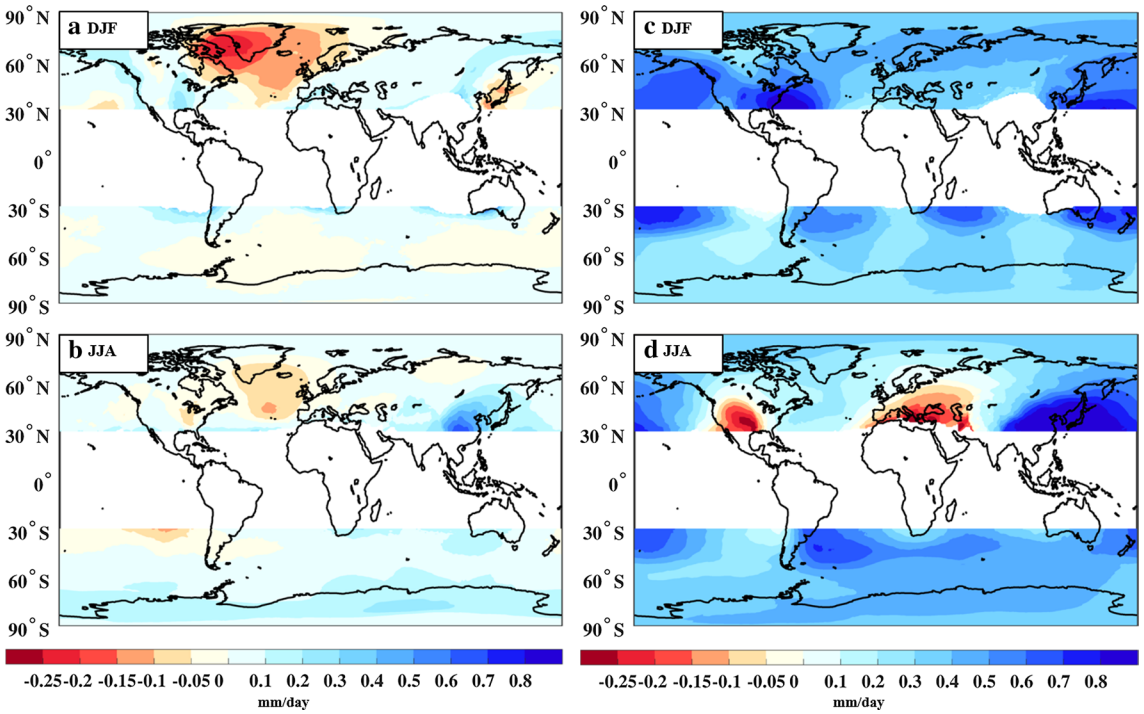

Fig. 12 Contributions to mean cyclone-wide averaged precipitation (⟨PR⟩) changes in the far-future (2081–2100). **a** DJF dynamic contributions, **b** JJA dynamic contributions, **c** DJF thermodynamic contributions, **d** JJA thermodynamic contributions. These maps were produced by constructing *circles* of great radius 2000 km at every grid point and applying the decomposition procedure described in Sect. 2.2.3 to the set of V, WVP and PR values of cyclones located within each *circle* in each ensemble member. The ensemble-mean of the resulting values of the contributions are assigned to the corresponding central grid point

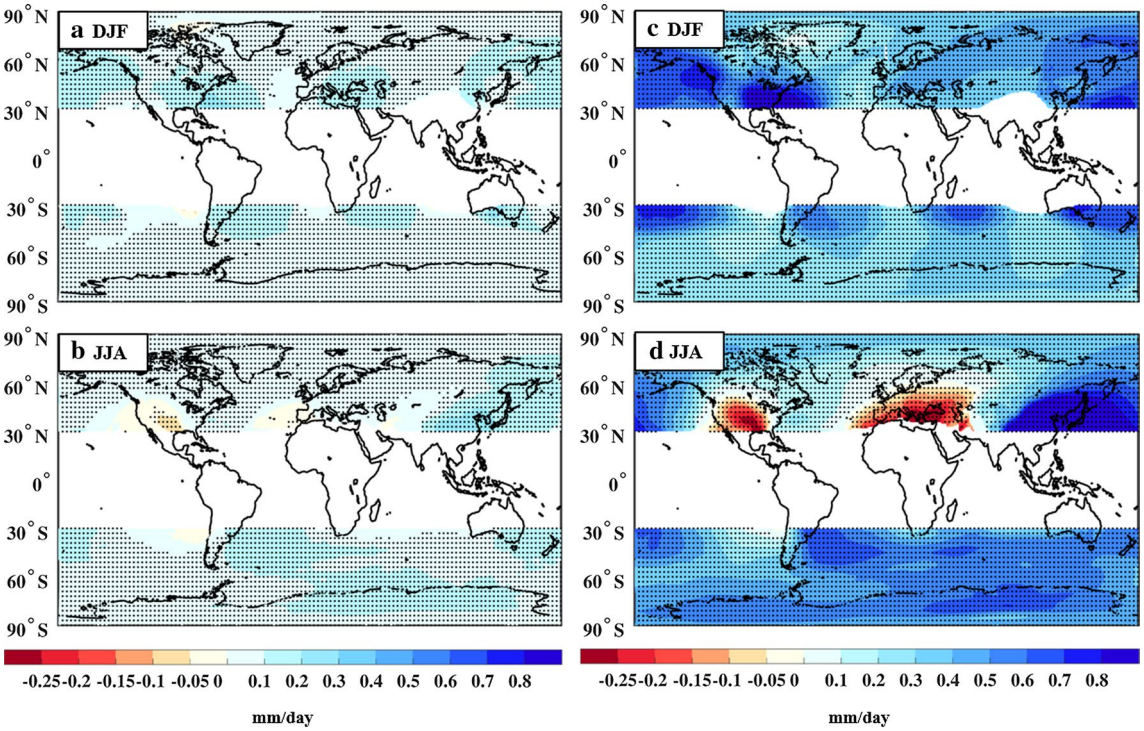

Fig. 13 Mean cyclonewide-averaged precipitation ⟨PR⟩ change: **a** DJF near-future (2016–2035) change, **b** JJA near-future change, **c** DJF far-future change (2081–2100) change, **d** JJA far-future change. Stippling indicates statistically significant change at the 95% confidence level

even on the regional scale (not shown) throughout the extratropics in both future periods. Our results imply that future cyclone change studies may be best served by focusing on their thermodynamic aspects. However, this does not eliminate the need to study changes in extremes of cyclonic winds due to their relevance to the society.

Like all studies, the methods applied here have limitations. This work assumes that cyclone V and WVP are independent quantities based on the arguments of Field and Wood (2007). Mathematically, this assumption translates to a negligible covariation term in Eq. 4. The covariation term was indeed found to be negligible when the decomposition of within cyclone precipitation changes into contributions from changes in cyclone V and WVP in the neighborhood of each grid point was performed taking into account complete sets of identified cyclones. When the decomposition was performed for particular cyclone strength regimes (e.g.: the middle tercile of a tercile-by-tercile partition of cyclones based on strength), the covariation term attained a magnitude comparable to the thermodynamic and dynamic terms. Cyclone thermodynamics and dynamics are coupled to each other in such a scenario and as a result the effect of their covariation must be included in the analysis.

Another limitation of this work is the use of daily averaged data. Because cyclones evolve on sub-daily timescales, the use of daily data smooths cyclones. For example, a side analysis shows that the precipitation maximum near cyclone centers was smaller in 24-hourly averaged composites than in 6-hourly averaged composites by as much 6 mm/day. While the use of daily data does affect the magnitude of the precipitation fields, the use of daily data does not change the fundamental conclusion of this work: thermodynamics dominate over dynamics. Our conclusion that the dynamics changes within cyclones are relatively small is consistent with idealized model experiments (Booth et al. 2013) and reanalysis data (Li et al. 2014).

Finally, we use an imperfect model with precipitation biases. Biases in the simulation of present-day precipitation imprint themselves on the projections of precipitation change since precipitation changes associated with warming correlate with the present-day pattern of precipitation (Bony et al. 2013). Although models represent front occurrence frequency well, they overestimate the frequency of frontal precipitation and underestimate its intensity (Catto et al. 2015). These compensating factors add little bias to accumulated precipitation and as a result, frontal precipitation is well represented on average in models. For example, using a cyclone-compositing approach, Field et al. (2008) have shown that accumulated cyclonic precipitation rate and composite structure over oceans reproduced by CAM are in good agreement with satellite estimates. However, the underestimation of frontal precipitation intensity could impact present-day simulations and future projections of model cyclone strength through the resulting underestimation of latent heat fluxes. Willison et al. (2013) argue that one cause of this deficiency could be the coarse resolution of present day GCMs. Horizontal resolution can have an important impact on storm track response to changes in large scale conditions such as moisture and dynamics. For example, Willison et al. (2013) show an enhanced positive feedback between cyclone intensification and latent heat release within the cyclone at higher resolutions, resulting in stronger storms relative to coarser simulations. As demonstrated by Govekar et al. (2014) and Field et al. (2008), model resolution can also impact the sensitivity of changes in model cyclonic clouds and precipitation to changes in moisture and dynamics. Specific to our study, Field et al. (2008) argue that Eq. (3) may not completely explain the variance seen in the model composite-mean rainfall rates which could potentially affect the quantitative decomposition results presented in Table 1. While important to consider, we do not think these factors change the essential conclusion of our work: changes in thermodynamics in a warming world explain most of the changes in cyclone precipitation.

5 Summary

Using a cyclone-compositing approach, we find that precipitation within extratropical cyclones as represented by a state-of-the-art global coupled climate model (CESM1-CAM5) increases in the future. With some regional exceptions, within-cyclone precipitation increases mostly due to increase in the cyclonic water vapor content, not changes in cyclonic wind speeds. Cyclone-associated precipitation increases mostly due to within-cyclone precipitation enhancement. Despite their potential to affect cyclone-associated precipitation, changes in cyclone frequency play only a secondary role with some regional exceptions. In spite of the potential for uncertainty arising from complex interaction of various physical drivers of change, internal climate variability has a negligible effect on the dominance of thermodynamic contributions to extratropical cyclone precipitation change over other controls on precipitation in the near- and far-futures.

Acknowledgements The authors wish to thank Isla Simpson for fruitful conversations related to this work, the Yellowstone CESM CSL for computing resources, and the scientists and software engineers that build CESM. This work was funded by start-up funds awarded to J. E. Kay by the University of Colorado Cooperative Institute for Research in Environmental Sciences (CIRES).

Appendix: Construction of cyclone-centric radial grids

The radial grids used in our study are centered on cyclone centers and consist of equally-spaced shells on the sphere

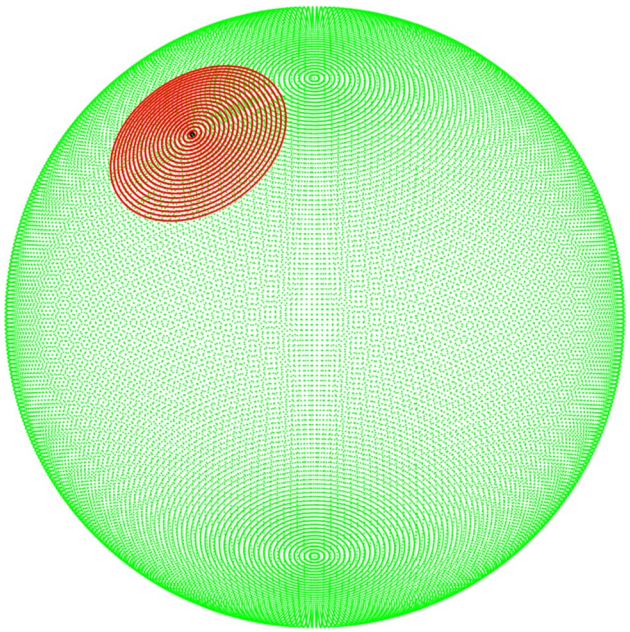

Fig. 14 Illustration of a cyclone-centric radial grid. The *green points* represent model grid points. The *black dot* is a sample cyclone center. The *red points* represent the radial grid

with each shell consisting of a desired number of points (Fig. 14).

Such radial grids have previously been used in Bengtsson et al. (2009) for cyclone compositing purposes. Here we give direct formulas for the construction of such grids.

Consider a cyclone center C identified on the globe at latitude ϕ and longitude λ where the angles are expressed in radians. The unit vectors $\overrightarrow{e_1}$, $\overrightarrow{e_2}$, $\overrightarrow{e_3}$ at C in the zonal, meridional and radial directions (assuming the center of the Earth to be the origin) respectively are given by

$$\overrightarrow{e_1} = -\sin(\lambda)\widehat{i} + \cos(\lambda)\widehat{j}$$

$$\overrightarrow{e_2} = -\sin(\phi)\cdot\cos(\lambda)\widehat{i} - \sin(\phi)\sin(\lambda)\widehat{j} + \cos(\phi)\widehat{k}$$

$$\overrightarrow{e_3} = \cos(\phi)\cdot\cos(\lambda)\widehat{i} + \cos(\phi)\sin(\lambda)\widehat{j} + \sin(\phi)\widehat{k}$$

where $\widehat{i}$, $\widehat{j}$, $\widehat{k}$ are the unit vectors of a fixed right-handed coordinate system with origin at the center of the globe.

Let s be the desired great-circle distance between the shells of the radial grid centered on C and m be the desired number of shells. Let the desired number of points on each shell be n. Then, the projections x, y, z of the radial vector joining the origin to the qth point on the pth shell are given by

$$x\widehat{i} + y\widehat{i} + z\widehat{k} = R\sin\left(\frac{ps}{R}\right)\cos\left(\frac{2\pi q}{n}\right)\overrightarrow{e_1} + R\sin\left(\frac{ps}{R}\right)\sin\left(\frac{2\pi q}{n}\right)\overrightarrow{e_2} + R\cos\left(\frac{2\pi q}{n}\right)\overrightarrow{e_3}$$

where R is the radius of the Earth, p can range from 1, 2, 3,…, m and q from 1,2,3,… n

The latitude and longitude $\phi_{p,q}$ and $\lambda_{p,q}$ of the point are then given by

$$\phi_{p,q} = \left(\frac{\pi}{2} - \arccos\left(\frac{z}{\sqrt{x^2+y^2+z^2}}\right)\right)\frac{180}{\pi}$$

$$\lambda_{p,q} = ((Arg(x+iy))mod(2\pi))\frac{180}{\pi}$$

where *mod* is the modulus operator, *Arg* stands for complex argument and i is the imaginary unit. $\phi_{p,q}$ and $\lambda_{p,q}$ are output in degrees, and lie in [−90, 90] and [0, 360) respectively. By iterating p and q from 1 to m and 1 to n respectively, the latitudes and longitudes of all radial grid points can be obtained.

References

Barnes EA, Polvani L (2013) Response of the midlatitude jets, and of their variability, to increased greenhouse gases in the CMIP5 models. J Clim 26:7117–7135. doi:10.1175/JCLI-D-12-00536.1

Bauer M, Del Genio AD (2006) Composite analysis of winter cyclones in a GCM: influence on climatological humidity. J Clim 19:1652–1672. doi:10.1175/JCLI3690.1

Bengtsson L, Hodges KI, Esch M, Keenlyside N, Kornblueh L, Luo JJ, Yamagata T (2007) How may tropical cyclones change in a warmer climate? Tellus Ser A Dyn Meteorol Oceanogr 59:539–561. doi:10.1111/j.1600-0870.2007.00251.x

Bengtsson L, Hodges KI, Keenlyside N (2009) Will extratropical storms intensify in a warmer climate? J Clim 22:2276–2301. doi:10.1175/2008JCLI2678.1

Blackmon ML (1976) A climatological spectral study of the 500 mb geopotential height of the Northern Hemisphere. J Atmos Sci 33:1607–1623. doi:10.1175/1520-0469(1976)033<1607:ACSSOT>2.0.CO;2

Bodas-Salcedo A, Williams KD, Field PR, Lock AP (2012) The surface downwelling solar radiation surplus over the southern ocean in the met office model: the role of midlatitude cyclone clouds. J Clim 25:7467–7486. doi:10.1175/JCLI-D-11-00702.1

Bony S, Dufresne J-L, Le Treut H, Morcrette J-J, Senior C (2004) On dynamic and thermodynamic components of cloud changes. Clim Dyn 22:71–86. doi:10.1007/s00382-003-0369-6

Bony S, Bellon G, Klocke D, Sherwood S, Fermepin S, Denvil S (2013) Robust direct effect of carbon dioxide on tropical circulation and regional precipitation. Nat Geosci 6:447–451. doi:10.1038/ngeo1799

Booth JF, Wang S, Polvani L (2013) Midlatitude storms in a moister world: lessons from idealized baroclinic life cycle experiments. Clim Dyn 41:787–802. doi:10.1007/s00382-012-1472-3

Catto JL, Jakob C, Berry G, Nicholls N (2012) Relating global precipitation to atmospheric fronts. Geophys Res Lett 39:1–6. doi:10.1029/2012GL051736

Catto JL, Jakob C, Nicholls N (2015) Can the CMIP5 models represent winter frontal precipitation? Geophys Res Lett 42:8596–8604. doi:10.1002/2015GL066015

Chang EKM, Guo Y, Xia X (2012) CMIP5 multimodel ensemble projection of storm track change under global warming. J Geophys Res Atmos 117:1–19. doi:10.1029/2012JD018578

Chang EKM, Zheng C, Lanigan P, Yau AMW, Neelin JD (2015) Significant modulation of variability and projected change in California winter precipitation by extratropical cyclone activity. Geophys Res Lett 42:5983–5991. doi:10.1002/2015GL064424

Emori S, Brown SJ (2005) Dynamic and thermodynamic changes in mean and extreme precipitation under changed climate. Geophys Res Lett 32:1–5. doi:10.1029/2005GL023272

Field PR, Wood R (2007) Precipitation and cloud structure in midlatitude cyclones. J Clim 20:233–254. doi:10.1175/JCLI3998.1

Field PR, Gettelman A, Neale RB, Wood R, Rasch PJ, Morrison H (2008) Midlatitude cyclone compositing to constrain climate model behavior using satellite observations. J Clim 21:5887–5903. doi:10.1175/2008JCLI2235.1

Finnis J, Holland MM, Serreze MC, Cassano JJ (2007) Response of Northern Hemisphere extratropical cyclone activity and associated precipitation to climate change, as represented by the community climate system model. J Geophys Res Biogeosci 112:1–14. doi:10.1029/2006JG000286

Fyfe JC (2003) Extratropical Southern Hemisphere cyclones: harbingers of climate change? J Clim 16:2802–2805. doi:10.1175/1520-0442(2003)016<2802:ESHCHO>2.0.CO;2

Govekar PD, Jakob C, Catto J (2014) The relationship between clouds and dynamics in Southern Hemisphere extratropical cyclones in the real world and a climate model. J Geophys Res Atmos 119:6609–6628. doi:10.1002/2013JD020699

Harvey BJ, Shaffrey LC, Woollings TJ, Zappa G, Hodges KI (2012) How large are projected 21st century storm track changes. Geophys Res Lett 39:1–5. doi:10.1029/2012GL052873

Hawcroft MK, Shaffrey LC, Hodges KI, Dacre HF (2012) How much Northern Hemisphere precipitation is associated with extratropical cyclones? Geophys Res Lett 39:1–7. doi:10.1029/2012GL053866

Held IM, Soden BJ (2006) Robust responses of the hydrological cycle to global warming. J Clim 19:5686–5699. doi:10.1175/JCLI3990.1

Hoskins BJ, Hodges KI (2005) A new perspective on Southern Hemisphere storm tracks. J Clim 18:4108–4129. doi:10.1175/JCLI3570.1

Hurrell JW et al (2013) The community earth system model: a framework for collaborative research. Bull Am Meteorol Soc 94:1339–1360. doi:10.1175/BAMS-D-12-00121.1

Kay JE et al (2015) The community earth system model (CESM) large ensemble project: a community resource for studying climate change in the presence of internal climate variability. Bull Am Meteorol Soc 96:1333–1349. doi:10.1175/BAMS-D-13-00255.1

Klein SA, Jakob C (1999) Validation and sensitivities of frontal clouds simulated by the ECMWF model. Mon Weather Rev 127:2514–2531. doi:10.1175/1520-0493(1999)127<2514:VASOFC>2.0.CO;2

Lambert SJ, Fyfe JC (2006) Changes in winter cyclone frequencies and strengths simulated in enhanced greenhouse warming experiments: results from the models participating in the IPCC diagnostic exercise. Clim Dyn 26:713–728. doi:10.1007/s00382-006-0110-3

Lau N-C, Crane MW (1995) A satellite view of the synoptic-scale organization of cloud properties in midlatitude and tropical circulation systems. Mon Weather Rev 123:1984–2006

Li M, Woollings T, Hodges K, Masato G (2014) Extratropical cyclones in a warmer, moister climate: a recent Atlantic analogue. Geophys Res Lett 41:8594–8601. doi:10.1002/2014GL062186

Naud CM, Posselt DJ, Van Den Heever SC (2012) Observational analysis of cloud and precipitation in midlatitude cyclones: Northern versus Southern hemisphere warm fronts. J Clim 25:5135–5151. doi:10.1175/JCLI-D-11-00569.1

Neu U et al (2013) Imilast: a community effort to intercompare extratropical cyclone detection and tracking algorithms. Bull Am Meteorol Soc 94:529–547. doi:10.1175/BAMS-D-11-00154.1

Pfahl S, Sprenger M (2016) On the relationship between extratropical cyclone precipitation and intensity. Geophys Res Lett. doi:10.1002/2016GL068018

Polvani LM, Previdi M, Deser C (2011) Large cancellation, due to ozone recovery, of future Southern Hemisphere atmospheric circulation trends. Geophys Res Lett 38:1–6. doi:10.1029/2011GL046712

Power SB, Delage F, Colman R, Moise A (2012) Consensus on twenty-first-century rainfall projections in climate models more widespread than previously thought. J Clim 25:3792–3809. doi:10.1175/JCLI-D-11-00354.1

Serreze MC (1995) Climatological aspects of cyclone development and decay in the Arctic. Atmos Ocean 33:1–23. doi:10.1080/07055900.1995.9649522

Tebaldi C, Knutti R (2007) The use of the multi-model ensemble in probabilistic climate projections. Philos Trans A Math Phys Eng Sci 365:2053–2075. doi:10.1098/rsta.2007.2076

Willison J, Robinson WA, Lackmann GM (2013) The importance of resolving mesoscale latent heating in the North Atlantic storm track. J Atmos Sci 70:2234–2250. doi:10.1175/JAS-D-12-0226.1

Woollings T, Hannachi A, Hoskins B (2010) Variability of the North Atlantic eddy-driven jet stream. Q J R Meteorol Soc 136:856–868. doi:10.1002/qj.625

Yin JH (2005) A consistent poleward shift of the storm tracks in simulations of 21st century climate. Geophys Res Lett 32:1–4. doi:10.1029/2005GL023684

Zappa G, Shaffrey LC, Hodges KI, Sansom PG, Stephenson DB (2013) A multimodel assessment of future projections of North Atlantic and European extratropical cyclones in the CMIP5 climate models. J Clim 26:5846–5862. doi:10.1175/JCLI-D-12-00573.1

Zappa G, Hawcroft MK, Shaffrey L, Black E, Brayshaw DJ (2014) Extratropical cyclones and the projected decline of winter Mediterranean precipitation in the CMIP5 models. Clim Dyn. doi:10.1007/s00382-014-2426-8